centre (carbene) or localized on two different atoms within the molecule (diradical). One of the best known reactions of triplet carbenes is their interaction with oxygen to form the corresponding ketones, which involves carbonyl oxide formation. In contrast, diradicals react with oxygen to give oxidation products mainly derived from the corresponding peroxides. When **1b** was irradiated in the presence of oxygen, bis [9-(10-phenyl)anthryl]ketone was formed. Laser flash photolysis studies showed the presence of a broad transient absorption at 505 nm ascribable to the carbonyl oxide. Moreover, whereas ^{3}**2a** aggregated into a trimer, ^{3}**2b** produced a carbene dimer (**4**) through coupling of two molecules at their carbene centres. These observations, and the fact that we observed the main decay pathway of persistent triplet carbenes in solution to be dimerization, suggest that even though the free electrons in ^{3}**2b** are extensively delocalized, it is considered more appropriately as a carbene than a diradical.

Although the conceptual ideas underpinning this work were developed more than a century ago, the present findings may still affect modern materials science because triplet carbene units can serve as a useful source of electron spins in high-spin organic molecules that act as models for purely organic ferromagnetics[29]. To date, the highly transient nature of these species has prevented further development of such systems into usable magnetic materials, but the relatively stable triplet carbene described here may point to new strategies for developing organic ferromagnetic materials. □

Received 5 March; accepted 4 June 2001.

1. Gomberg, M. Triphenylmethyl, ein Fall von dreiwerthigem Kohlenstoff. *Ber. Deutsch. Chem. Ges.* **33,** 3150–3163 (1900).
2. Gomberg, M. An instance of trivalent carbon: Triphenylmethyl. *J. Am. Chem. Soc* **22,** 757–771 (1900).
3. Staudinger, H. & Kupfer, O. Über Reaktionen des Methylenes. Diazomethan. *Ber. Deutsch. Chem. Ges.* **45,** 501–509 (1912).
4. Hine, J. Carbon dichloride as an intermediate in basic hydrolysis of chloroform. A mechanism for substitution reactions at a saturated carbon atom. *J. Am. Chem. Soc.* **72,** 2438–2445 (1950).
5. Doering, W. v. E. & Hoffmann, A. K. Addition of dichlorocarbene to olefins. *J. Am. Chem. Soc.* **76,** 6162–6165 (1954).
6. Igau, A., Grützmacher, H., Baceiredo, A. & Bertrand, G. Analogous α,α′–bis-carbenoid triply bonded species: Synthesis of a stable λ^3-phosphinocarbene-λ^5-phosphaacetylene. *J. Am. Chem. Soc.* **110,** 6463–6466 (1988).
7. Arduengo, A. J. III, Harlow, R. L. & Kline, M. A stable crystalline carbene. *J. Am. Chem. Soc.* **113,** 361–363 (1991).
8. Bourissou, D., Guerret, O., Gabbäi, F. P. & Bertrand, G. Stable carbenes. *Chem. Rev* **100,** 39–91 (2000).
9. Arduengo, A. J. III. Looking for stable carbenes: The difficulty in starting anew. *Acc. Chem. Res.* **32,** 913–921 (1999).
10. Regitz, M. Stable carbenes—illusion or reality. *Angew. Chem. Int. Edn Engl.* **30,** 674–676 (1991).
11. Dagani, R. Preparation of stable divalent species raises issues of electronic structure. *Chem. Eng. News* **2,** 20–22 (1994).
12. Heinemann, C., Müller, T., Apeloig, A. & Schwartz, H. On the question of stability, conjugation, and "aromaticity" in imidazol-2-ylidenes and their silicon analogs. *J. Am. Chem. Soc.* **118,** 2023–2038 (1996).
13. Kirmse, W. (ed.) *Carbene Chemistry* 159–504 2nd edn (Academic, New York, 1971).
14. Jones, M & Moss, R. M. (eds) *Carbenes* Vol. II, 159–362 (Wiley, New York, 1975).
15. Tomioka, H. Persistent triplet carbenes. *Acc. Chem. Res.* **30,** 315–321 (1997).
16. Tomioka, H. Persistent triplet carbenes. *Adv. Carbene Chem.* **2,** 175–214 (1998).
17. Hirai, K. & Tomioka, H. A triplet carbene that can almost be bottled. *J. Am. Chem. Soc.* **121,** 10213–10214 (1999).
18. Murray, R. W., Trozzolo, A. M., Wasserman, E. & Yager, W. A. E.p.r. of diphenylmethylene, a ground-state triplet. *J. Am. Chem. Soc.* **84,** 3213–3214 (1962).
19. Itoh, K. Electron spin resonance of an aromatic hydrocarbon in its quintet ground state. *Chem. Phys. Lett.* **1,** 235–238 (1969).
20. Bandon, R. W., Closs, G. & Hutchison, C. A. Jr. Paramagnetic resonance in oriented ground-state triplet molecules. *J. Chem. Phys.* **37,** 1878–1879 (1962).
21. Sander, W., Bucher, G. & Wierlacher, S. Carbenes in matrices—spectroscopy, structure, and reactivity. *Chem. Rev.* **93,** 1583–1621 (1993).
22. Wasserman, E. *et al.* Electron paramagnetic resonance of 9,9′-dianthrylmethylene. A linear aromatic ground-state triplet methylene. *J. Am. Chem. Soc.* **93,** 6335–6337 (1971).
23. Astles, D. S. *et al.* The unusual reactivity of 9,9′-dianthrylcarbene. *J. Org. Chem.* **53,** 6053–6057 (1988).
24. Takahashi, Y. *et al.* Triplet di(9-anthryl)carbene undergoes trimerization. *Angew. Chem. Int. Edn Engl.* **39,** 3478–3480 (2000).
25. Tomioka, H. Strain and structure of sterically congested triplet carbenes. *Adv. Strained Interesting Organic Mol.* **8,** 83–112 (2000).
26. Gibbons, W. A. & Trozzolo, A. M. Spectroscopy and photolysis of a ground-state triplet molecule, diphenylmethylene. *J. Am. Chem. Soc.* **88,** 172–173 (1966).
27. Moritani, I., Murahashi, S.-I., Nishino, M., Kimura, K. & Tsubomura, H. Electronic spectra of the products formed by the photolysis of diazo compound at 77 K, possibly identified to carbenes. *Tetrahedr. Lett.* **4,** 373–378 (1966).
28. Closs, G., Hutchison, C. A. & Kohler, B. E. Optical absorption spectra of substituted methylenes oriented in single crystals. *J. Chem. Phys.* **44,** 413–414 (1966).
29. Iwamura, H. High-spin organic molecules and spin alignment in organic molecular assemblies. *Adv. Phys. Org. Chem.* **26,** 179–253 (1990).

Supplementary information is available on *Nature*'s World-Wide Web site (http://www.nature.com) or as paper copy from the London editorial office of *Nature*.

Acknowledgements

We thank A. Nicolaides for critical reading of the manuscript. This work was supported by a Grant-in-Aid for Specially Promoted Research from the Ministry of Education, Science, Culture and Sports of Japan, the Nagase Science and Technology Foundation and the Mitsubishi Foundation.

Correspondence and requests for materials should be addressed to H.T. (e-mail: tomioka@chem.mie-u.ac.jp).

Normal faulting in central Tibet since at least 13.5 Myr ago

Peter M. Blisniuk*, Bradley R. Hacker†, Johannes Glodny‡, Lothar Ratschbacher§, Siwen Bi‖, Zhenhan Wu‖, Michael O. McWilliams¶ & Andy Calvert†

* *Institut für Geowissenschaften, Universität Potsdam, D-14415 Potsdam, Germany*
† *Department of Geological Sciences, University of California, Santa Barbara, California 93106, USA*
‡ *GeoForschungsZentrum Potsdam, D-14473 Potsdam, Germany*
§ *Institut für Geologie, Technische Universität Bergakademie Freiberg, D-09596 Freiberg, Germany*
‖ *Institute of Geomechanics, Chinese Academy of Geological Sciences, Beijing 100081, China*
¶ *Department of Geology and Environmental Sciences, Stanford University, Stanford, California 94305, USA*

Tectonic models for the evolution of the Tibetan plateau interpret observed east–west thinning of the upper crust to be the result of either increased potential energy of elevated crust[1] or geodynamic processes that may be unrelated to plateau formation[2–6]. A key piece of information needed to evaluate these models is the timing of deformation within the plateau. The onset of normal faulting has been estimated to have commenced in southern Tibet between about 14 Myr ago[7] and about 8 Myr ago[8] and, in central Tibet, about 4 Myr ago[9]. Here, however, we report a minimum age of approximately 13.5 Myr for the onset of graben formation in central Tibet, based on mineralization ages determined with Rb–Sr and ^{40}Ar–^{39}Ar data that post-date a major graben-bounding normal fault. These data, along with evidence for prolonged activity of normal faulting in this and other Tibetan grabens, support models that relate normal faulting to processes occurring beneath the plateau. Thinning of the upper crust is most plausibly the result of potential-energy increases resulting from spatially and temporally heterogeneous changes in thermal structure and density distribution within the crust and upper mantle beneath Tibet. This is supported by recent geophysical and geological data[10–17], which indicate that spatial heterogeneity exists in both the Tibetan crust and lithospheric mantle.

The Tibetan plateau consists of several continental fragments (Fig. 1a) that were accreted to the southern margin of Eurasia during the Palaeozoic and Mesozoic eras. Although crustal thickening due to these collisions may have raised portions of the plateau[18], most of the plateau's current elevation is attributed to the India–

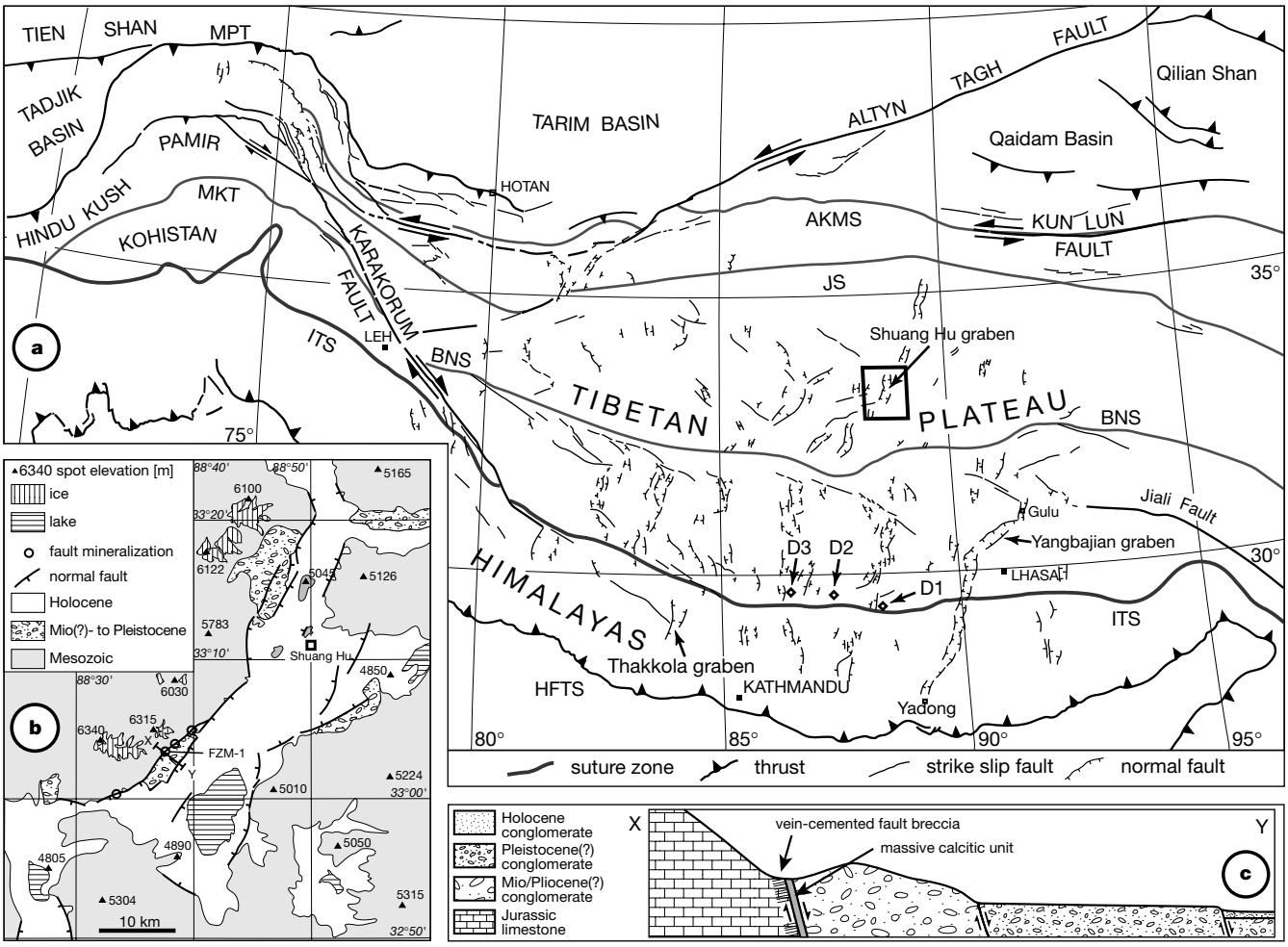

Figure 1 Geological setting of the studied normal fault mineralization. **a**, Generalized tectonic overview map of the Himalaya–Tibet orogen, showing major fault zones with late Cenozoic displacements, and suture zones bordering (and within) the Tibetan plateau. Abbreviations are: AKMS, Ayimaqin–Kunlun–Mutztagh suture; BNS, Bangong–Nujiang suture; HFTS, Himalayan frontal thrust system; ITS, Indus–Tsangpo suture; JS, Jinsha suture; MKT, main Karakorum thrust; MPT, main Pamir thrust. D1 indicates location of dyke dated at ~18 Myr ago[2], D2 and D3 are locations of dykes dated at ~18 to ~13 Myr ago[22]. The Lhasa block is located between the ITS and the BNS, the Qiangtang block between the BNS and the JS. **b**, Generalized geological overview map of Shuang Hu graben (for location, see frame in **a**). **c**, Schematic cross-section of normal fault zone at locality FZM-1 along the western margin of Shuang Hu graben (for location, see line X–Y on **b**).

Eurasia collision. Elevation changes cannot be dated directly, but a widely held view is that the onset of normal faulting on the plateau, which extracts potential energy from the crust beneath the plateau, records the time when the maximum elevation of the plateau had been reached[1]. A popular hypothesis supporting this view relates uplift of the plateau to convective thinning of its lithospheric root[19]. But other models, interpreting normal faulting as a consequence of uplift achieved through other processes, or as unrelated to uplift, are also geodynamically sensible (see refs 2 and 20 for reviews).

Dating the onset of normal faulting on the plateau is a crucial test of the validity of these models, but very few published studies have provided reliable age constraints in this region (Fig. 1a): near the southern margin of the plateau, a minimum age for significant east–west crustal thinning by normal faults of the Thakkola graben is ~11 Myr, based on the oldest fault-related sediments observed[21]. Mineralized north–south-trending fractures near the graben dated at ~14 Myr indicate at least minor east–west stretching during their formation, and may correlate to normal faulting in the graben[7]. Within the south Tibetan Lhasa block, the onset of significant east–west extension along a low-angle normal fault bounding the Yangbajian graben is dated at 8 ± 1 Myr[8]. However, north–south-trending dykes, about 18–13 Myr old, in the Lhasa block indicate that at least minor east–west stretching dates back to approximately 18 Myr (refs 2, 22). In the central Tibetan Qiangtang block, the integration of estimates for the Holocene slip rate with the total slip of a major graben-bounding normal fault in the Shuang Hu graben has been used to infer an age of ~4 Myr for the initiation of extension[9].

The data we report here also result from a study of the NNE-trending Shuang Hu graben, ~50 km long and 10 km wide, in the central Tibetan Qiangtang block (Fig. 1). The vertical offset along the structurally dominant western graben margin has been estimated at ~7 km (ref. 9). The stratigraphy is dominated by Mesozoic strata on the graben shoulders, and Holocene deposits covering the graben floor[9]. The oldest observed deposits interpreted as graben fill are undated coarse conglomerates exposed locally on fault blocks (Fig. 1b, c). Along both graben margins, Quaternary terraces and fans are offset by active normal faults with prominent fault scarps. The geometry of extension in the Shuang Hu graben is constrained by slip directions on minor faults in major graben-bounding normal fault zones striking 020–050° and dipping 50–80° to the east. Kinematic analysis of these data, to be presented in detail elsewhere, indicates that the orientation of extension is ~120°. This agrees well with overall structural patterns and fault plane solutions

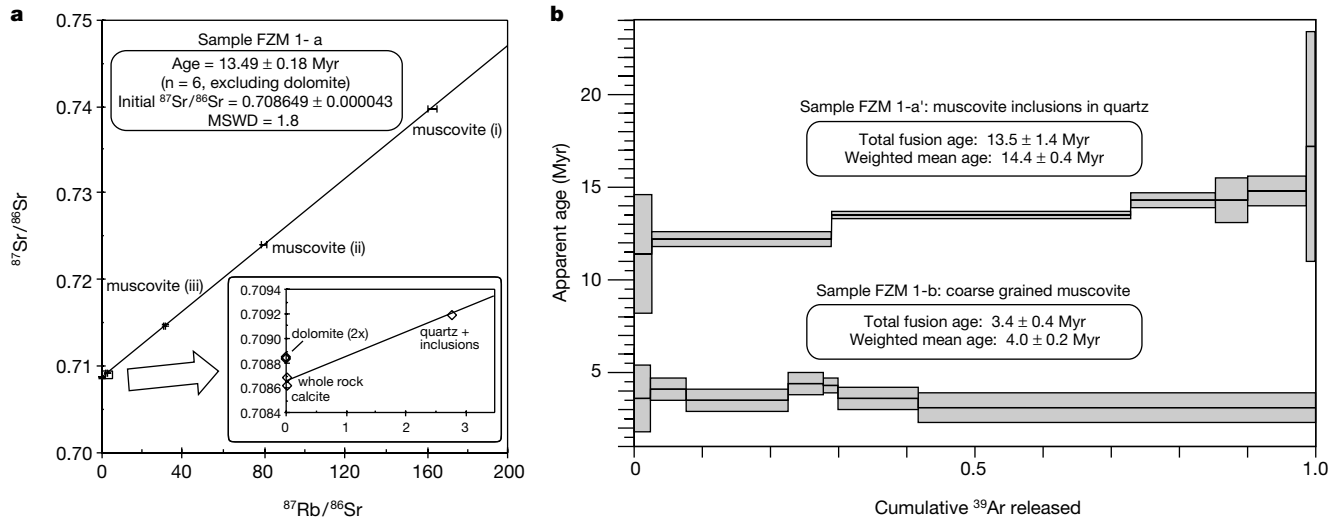

Figure 2 Results of isotope dating. **a**, Rb–Sr data of mineral assemblage from sample FZM 1-a. For meaning of muscovites (i), (ii) and (iii), see Table 1. Dolomite was excluded from the age calculation as it may be secondary. Microtextures suggest that the analysed minerals were not strictly syngenetic, but crystallized in subsequent stages of hydrothermal activity. This is reflected in the isotopic data by a slight non-analytical scatter around the regression line, and by the Sr isotopic disequilibrium between dolomite and calcite. However, integration of the dolomite data in the regression does not change the age value significantly (13.43 ± 0.21 Myr, $n = 8$, mean square of weighted deviates (MSWD) is 24). **b**, Incremental Ar release spectra for muscovite-rich quartz from sample FZM 1-a, and for muscovite from FZM 1-b. Sample FZM 1-a′ yielded a sequence of serially increasing step ages, and has a total fusion age of 13.5 ± 1.4 Myr. Three of the highest temperature steps with the highest K/Ca ratios (26% of the total ^{39}Ar) give a mean age weighted by age uncertainty of 14.4 ± 0.4 Myr, and an inverse isochron age of 13.6 ± 0.9 Myr. The serially increasing step ages may be the result of (1) *in vacuo* inhomogeneous release of ^{40}Ar and ^{39}Ar, in which case the total fusion age of the sample could be considered ''best''; (2) two crystallization events, at ~14.8 Myr and ~12.5 Myr; or (3) a continuum of Ar retention from growth during crystallization at 14.8 to 12.5 Myr. The simplest interpretation, consonant with the Rb–Sr age, is that the total fusion age represents mica crystallization. For muscovite from sample FZM 1-b, the individual laser ages are not internally concordant, low in radiogenic yield, and range from 3.1 to 4.4 Myr. A weighted mean of all seven laser step ages is 4.0 ± 0.2 Myr (MSWD = 2.3). All errors indicated are 2σ.

of earthquakes[23], implying that the Shuang Hu graben is a typical extensional structure of central Tibet.

A minimum age for the onset of important east–west extension in the Shuang Hu graben is recorded by mineralization in the main graben-bounding normal fault zone. At four locations (Fig. 1b) we observed a massive, 2–8-m-thick, calcite-dominated unit along the fault, separating vein-cemented fault breccia of adjacent (probably Jurassic) rocks of the graben shoulder in the west, and (probably Miocene) conglomerates on the fault block to the east (Fig. 1c). At three of the four localities, tufa deposits and mineralized springs occur. At each of the studied sites, the mineralized unit is laterally continuous over tens to hundreds of metres before disappearing under alluvium. Consequently, the mineralized unit appears to be of significant lateral extent, and its emplacement along the fault clearly demonstrates that it post-dates the onset of graben formation.

The fault zone mineralization consists of coarse-grained, non-porous calcite with rare accessory minerals. The investigated rock, from locality FZM-1 (Fig. 1b, c), contains fractures and minor shear planes parallel to the main fault plane, with a typical spacing of ~10 cm. Along these, the rock is altered and contains abundant muscovite. Realizing that mineralization may have been diachronous, we separately processed and dated two portions of the sample. One (FZM 1-a) consisted of the unfractured dense portions of the rock. The other (FZM 1-b) contained relatively muscovite-rich bands and rinds associated with the fractures and shear planes.

The Rb–Sr isotope data for muscovite, quartz (with small muscovite, fluid and carbonate inclusions), calcite, and whole rock from sample FZM 1-a yielded an age of 13.5 ± 0.2 Myr (Table 1, Fig. 2a). As an independent test of this result, we performed ^{40}Ar–^{39}Ar analysis of quartz grains rich in muscovite inclusions from this sample. The apparent age spectrum implies that mineralization occurred at 13.5 ± 1.4 Myr, but a complex crystallization history starting at 14.4 ± 0.4 Myr is possible (Table 2, Fig. 2b). For muscovite from sample FZM 1-b, we obtained a mean ^{40}Ar–^{39}Ar age of 4.0 ± 0.2 Myr (Table 2, Fig. 2b). We interpret these geochronological data to reflect mineralization at or before 13.5 Myr, and a later stage of muscovite growth or deformation-induced ^{40}Ar loss at ~4 Myr.

These results show that normal faulting in the central Tibetan Shuang Hu graben started before ~13.5 Myr ago. Furthermore, the 13.5-Myr minimum age of normal faulting, the ~4-Myr age of late-stage mica growth or deformation-induced Ar loss, and significant

Table 1 Rb–Sr data for fault mineralization, Shuang Hu graben

Analysis no.	Material	Rb (p.p.m.)	Sr (p.p.m.)	^{87}Rb/^{86}Sr	^{87}Sr/^{86}Sr
PS131	Dolomite (single crystal)	0.35	335.05	0.0030	0.708846 ± 11
PS91	Dolomite (replicate)	0.30	320.41	0.0027	0.708834 ± 13
PS130	Calcite (single crystal)	0.09	795.00	0.0003	0.708618 ± 13
PS54	Muscovite (i)	450.20	8.03	162.6741	0.739691 ± 16
PS57	Muscovite (ii)	443.38	16.12	79.7035	0.724036 ± 12
PS55a	Muscovite (iii)	432.32	39.89	31.3767	0.714629 ± 11
PS53	Quartz + inclusions, leached (iv)	29.63	30.91	2.7733	0.709188 ± 10
PS68	Whole rock	3.74	855.74	0.0126	0.708678 ± 11

These data are from sample FZM 1-a, analysed at GeoForschungsZentrum Potsdam. Muscovite (i), >100 μm, treated with acetic acid (25%) then oxalic acid (5%); muscovite (ii), >100 μm, treated with acetic acid (25%); muscovite (iii), >100 μm, no acid treatment; quartz + inclusions (iv), leached in hot aqua regia (3 h). Errors (2σ) for isochron calculation: ±1.5% for ^{87}Rb/^{86}Sr, ±0.005% for ^{87}Sr/^{86}Sr.

Table 2 ^{40}Ar–^{39}Ar data for hydrothermal muscovite, Shuang Hu graben

T (°C)	*t* (min)	^{40}Ar (10^{-15} mol)	$^{40}Ar/^{39}Ar$	$^{38}Ar/^{39}Ar$	$^{37}Ar/^{39}Ar$	$^{36}Ar/^{39}Ar$	K/Ca	$\Sigma^{39}Ar$ (%)	$^{40}Ar^*$	Age (Myr)
Sample FZM 1-a′										
550	12	8.00	66.1142	6.40×10^{-3}	0.1806	0.2018	2.7	2.58	0.098	11.4 ± 1.6
700	12	18.0	14.4979	0.00	0.4983	0.0255	0.98	28.93	0.481	12.2 ± 0.2
850	12	23.0	11.1971	0.00	0.2978	0.0119	1.6	72.89	0.687	13.5 ± 0.1
950	12	9.10	15.6349	0.00	0.3414	0.0252	1.4	85.27	0.524	14.3 ± 0.2
1,000	12	3.20	14.1738	0.00	0.2807	0.0204	1.7	90.00	0.574	14.3 ± 0.6
1,075	12	8.20	19.8975	0.00	0.2336	0.0388	2.1	98.71	0.424	14.8 ± 0.4
1,150	12	5.40	96.4782	0.00	1.7430	0.2931	0.28	99.90	0.102	17.2 ± 3.1
1,225	12	7.30	2130.2571	7.50×10^{-2}	23.6827	7.0862	0.021	99.97	0.017	62.7 ± 369.8
1,300	12	6.70	4751.1260	0.00	19.5559	16.0119	0.025	100.00	0.004	34.2 ± 1959.9
Sample FZM 1-b										
		9.7	54.9376	ND	0.2165	0.1297	2.3	2.39	0.302	3.6 ± 0.9
		21.0	52.6670	ND	0.1414	0.1149	3.5	7.64	0.355	4.1 ± 0.3
		58.0	52.2451	ND	0.0801	0.1231	6.1	22.61	0.304	3.5 ± 0.3
		19.0	50.5137	ND	0.1441	0.1038	3.4	27.75	0.392	4.4 ± 0.3
		8.4	52.4667	ND	0.2613	0.1116	1.9	29.92	0.371	4.3 ± 0.2
		46.0	52.0011	ND	0.0921	0.1210	5.3	41.73	0.312	3.6 ± 0.3
		210.0	48.0376	ND	0.1395	0.1142	3.5	100.00	0.298	3.1 ± 0.4

Sample FZM 1-a′: quartz grains rich in muscovite inclusions, hand-picked from the mineral separate used for Rb–Sr analysis, and analysed by step heating in a resistance furnace (UCSB), $J = 0.0009744$. Sample FZM 1-b: muscovite hand-picked from crushed rock and analysed by laser step-heating of groups of grains (Stanford University), $J = 0.0001216$ and $0.001218 \pm 0.5\%$. *J*, irradiation flux parameter; *T*, temperature of furnace; *t*, time in furnace at temperature *T*; ^{40}Ar, moles of ^{40}Ar corrected for blank and reactor-produced ^{40}Ar; $\Sigma^{39}Ar$, cumulative ^{39}Ar released; $^{40}Ar^*$, radiogenic fraction; ND, not determined. Ratios are corrected for blanks, decay, and interference; errors on age are $\pm 1\sigma$.

Quaternary normal faulting demonstrate prolonged upper-crustal thinning in that region. This is similar to the situation farther south on the Tibetan plateau. In the south Tibetan Lhasa block, north–south-trending dyke swarms indicate east–west stretching since ~18 Myr ago[2,22], and studies in the Yangbajian graben, formed ~8 Myr ago[8], have documented Quaternary and recent normal faulting[3]. In the Thakkola graben, normal faulting occurred in multiple phases from ~11 Myr into the Quaternary[24,25], and may have started as early as ~14 Myr ago[7].

The available age data, although not sufficient to resolve the chronology of Tibet's upper-crustal extension in detail, call into question the relevance of models relating Tibetan normal faulting to processes occurring near the margins of (or outside) the plateau. For example, mechanisms attributing normal faulting in southern Tibet to motion along the Karakorum–Jiali fault zone[3], to radial convergence[4], or to oroclinal bending[5,6] are not likely to have triggered significant extension in central Tibet, although they may have influenced its distribution in southern Tibet. A link between crustal thinning in Tibet and important regional normal faulting in north-central Asia (for example, Shanxi, Baikal)[2]—poorly dated, but thought to have initiated during latest Miocene to Early Pliocene times[26,27]—is also not supported by evidence for normal faulting in central and southern Tibet at or before 13.5 Myr ago. In contrast, the view that the onset of crustal thinning is related to increased potential energy of elevated crust is consistent with this evidence, and supported by palaeoelevation estimates for ~11-Myr-old Thakkola graben sediments that are similar to modern elevations on the plateau[21].

The most plausible causes for important potential-energy increases are changes in the thermal structure and density distribution within the crust and upper mantle beneath Tibet. Geophysical and geological evidence[10–17] indicates a heterogeneous crust and lithospheric mantle structure beneath Tibet—characterized, for example, by decreasing crustal thickness from south to north, hot upper crust but cold lower crust and lithospheric mantle in the south, and hot lower crust and lithospheric mantle in the north. This makes it difficult to interpret increased potential energy as being caused by the same process occurring simultaneously beneath the entire plateau, as has been suggested for convective removal of lower lithosphere[19]. It is more likely that the processes controlling potential-energy changes within the crust and upper mantle beneath Tibet have been heterogeneous spatially and temporally. In the interpretation that crustal thinning in Tibet is the result of increased potential energy of elevated crust, the few available age constraints on normal faulting imply high surface elevation in parts of southern and central Tibet, but not necessarily throughout the entire present-day plateau, by ~14 Myr ago. If important regional climate changes at ~8 Myr ago[28–30] were related to the evolution of the Tibetan plateau, they probably occurred after the plateau had attained a critical minimum elevation and/or size. It seems possible that the value of either one or both of these parameters increased between ~14 Myr and ~8 Myr ago. □

Received 30 January; accepted 22 June 2001.

1. Molnar, P. & Tapponnier, P. Active tectonics of Tibet. *J. Geophys. Res.* **83,** 5361–5375 (1978).
2. Yin, A. & Harrison, T. M. Geologic evolution of the Himalayan-Tibetan orogen. *Annu. Rev. Earth Planet. Sci. Lett.* **28,** 211–280 (2000).
3. Armijo, R., Tapponnier, P. & Han, T. Late Cenozoic strike-slip faulting in southern Tibet. *J. Geophys. Res.* **94,** 2787–2838 (1989).
4. Klootwijk, C. T., Conaghan, P. J. & Powell, C. M. The Himalayan arc: large-scale continental subduction, oroclinal bending and back-arc spreading. *Earth Planet. Sci. Lett.* **75,** 167–183 (1985).
5. McCaffrey, R. & Nabelek, J. Role of oblique convergence in the active deformation of the Himalayas and southern Tibet plateau. *Geology* **26,** 691–694 (1998).
6. Ratschbacher, L., Frisch, W., Lui, G. & Chen, C. Distributed deformation in southern and western Tibet during and after the India-Asia collision. *J. Geophys. Res.* **99,** 19917–19945 (1994).
7. Coleman, M. & Hodges, K. Evidence for Tibetan plateau uplift before 14 Myr ago from a new minimum age for east-west extension. *Nature* **374,** 49–52 (1995).
8. Harrison, T. M., Copeland, P., Kidd, W. S. F. & Lovera, O. M. Activation of the Nyainqentanghla Shear Zone: Implications for uplift of the southern Tibetan Plateau. *Tectonics* **14,** 658–676 (1995).
9. Yin, A. *et al.* Evidence for significant Late Cenozoic E-W extension in North Tibet. *Geology* **27,** 787–790 (1999).
10. Nelson, K. D. *et al.* An INDEPTH view of the structure of the lithosphere beneath southern Tibet. *Science* **274,** 1684–1688 (1996).
11. Owens, T. J. & Zandt, G. Implications of crustal property variations for models of Tibetan plateau evolution. *Nature* **387,** 37–43 (1997).
12. Kosarev, G. *et al.* Seismic evidence for a detached Indian lithospheric mantle beneath Tibet. *Science* **283,** 1306–1309 (1999).
13. Hacker, B. R. *et al.* Hot and dry deep crustal xenoliths from Tibet. *Science* **287,** 2463–2466 (2000).
14. Huang, W.-C. *et al.* Seismic polarization anisotropy beneath the central Tibetan Plateau. *J. Geophys. Res.* **105,** 27979–27989 (2000).
15. Wei, W. *et al.* Detection of widespread fluids in the Tibetan crust by magnetotelluric studies. *Science* **292,** 716–718 (2001).
16. Zhao, W. *et al.* Crustal structure of central Tibet as derived from project INDEPTH wide-angle seismic data. *Geophys. J. Int.* **145,** 486–498 (2001).
17. Rodgers, A. J. & Schwartz, S. Y. Lithospheric structure of the Qiangtang Terrane, northern Tibetan Plateau, from complete regional waveform modeling: Evidence for partial melt. *J. Geophys. Res.* **103,** 7137–7152 (1998).
18. England, P. & Searle, M. The Cretaceous-Tertiary deformation of the Lhasa Block and its implications for crustal thickening in Tibet. *Tectonics* **5,** 1–14 (1986).
19. England, P. C. & Houseman, G. A. Extension during continental convergence, with application to the Tibetan plateau. *J. Geophys. Res.* **94,** 17561–17579 (1989).
20. Harrison, T. M., Copeland, P., Kidd, W. S. F. & Yin, A. Raising Tibet. *Science* **255,** 1663–1670 (1992).
21. Garzione, C. N., Dettman, D. L., Quade, J., DeCelles, P. G. & Butler, R. F. High times on the Tibetan Plateau: Paleoelevation of the Thakkola graben, Nepal. *Geology* **28,** 339–342 (2000).
22. Williams, H., Turner, S., Kelley, S. & Harris, N. Age and composition of dikes in Southern Tibet: New constraints on the timing of east-west extension and its relationship to postcollisional volcanism. *Geology* **29,** 339–342 (2001).

23. Molnar, P. & Lyon-Caen, H. Fault plane solutions of earthquakes and active tectonics of the northern and eastern parts of the Tibetan Plateau. *Geophys. J. Int.* **99,** 123–153 (1989).
24. Hodges, K. V. *et al.* Simultaneous Miocene extension and shortening in the Himalayan orogen. *Science* **258,** 1466–1470 (1992).
25. Hurtado, J. M., Hodges, K. V. & Whipple, K. X. Neotectonics of the Thakkola graben and implications for recent activity on the South Tibetan fault system in the central Nepal Himalaya. *Bull. Geol. Soc. Am.* **113,** 222–240 (2001).
26. Zhang, Y., Vergely, P. & Mercier, J. L. Pliocene-Quaternary faulting pattern and left-slip propagation tectonics in North China. *Episodes* **22,** 84–88 (1999).
27. Logatchev, N. A. & Zorin, Y. A. Evidence and causes of the two-stage development of the Baikal rift. *Tectonophysics* **143,** 225–234 (1987).
28. Kroon, D., Steens, T. & Troelstra, S. R. Onset of monsoonal related upwelling in the western Arabian Sea as revealed by planktonic foraminifers. *Proc. ODP Sci. Res.* **116,** 257–263 (1991).
29. Quade, J., Cerling, T. E. & Bowman, J. R. Development of Asian monsoon revealed by marked ecological shift during the latest Miocene in northern Pakistan. *Nature* **342,** 163–166 (1989).
30. An, Z., Kutzbach, J. E., Prell, W. L. & Porter, S. C. Evolution of Asian monsoons and phased uplift of the Himalaya-Tibetan plateau since Late Miocene times. *Nature* **411,** 62–66 (2001).

Acknowledgements

We thank E. Gnos, M. Strecker, W. Kidd, A. Yin and M. Edwards for discussions, and P. Molnar for comments and suggestions. This work was supported by Deutsche Forschungsgemeinschaft, the US NSF, and the Chinese Academy of Geological Sciences.

Correspondence and requests for materials should be addressed to P.M.B. (e-mail: blisniuk@rz.uni-potsdam.de).

Resistance to mantle flow inferred from the electromagnetic strike of the Australian upper mantle

Fiona Simpson

Geophysics Institute, University of Göttingen, Germany, and Institute of Geological & Nuclear Sciences, 69 Gracefield Road, PO Box 30-368, Lower Hutt, New Zealand

Seismic anisotropy is thought to result from the strain-induced lattice-preferred orientation of mantle minerals, especially olivine[1,2], owing to shear waves propagating faster along the *a*-axis of olivine crystals than along the other axes. This anisotropy results in birefringence, or 'shear-wave splitting'[3], which has been investigated in numerous studies[1,4]. Although olivine is also anisotropic with respect to electrical conductivity[5] (with the *a*-axis being most conductive), few studies of the electrical anisotropy of the upper mantle have been undertaken, and these have been limited to relatively shallow depths in the lithospheric upper mantle[6,7]. Theoretical models of mantle flow have been used to infer that, for progressive simple shear imparted by the motion of an overriding tectonic plate, the *a*-axes of olivine crystals should align themselves parallel to the direction of plate motion[8,9]. Here, however, we show that a significant discrepancy exists between the electromagnetic strike of the mantle below Australia and the direction of present-day absolute plate motion[10]. We infer from this discrepancy that the *a*-axes of olivine crystals are not aligned with the direction of the present-day plate motion of Australia, indicating resistance to deformation of the mantle by plate motion.

Most studies of continental seismic anisotropy have been founded on analyses of the splitting of SKS shear waves. A disadvantage of this is the ambiguity associated with the depth at which anisotropy occurs. This has created a controversy, with some authors attributing seismic anisotropy to 'frozen-in' lithospheric anisotropy associated with palaeo-orogenic deformations[4,11], and others attributing it to sublithospheric anisotropy owing to strain-induced lattice-preferred orientation of olivine[1]. This ambiguity can be resolved to some extent using magnetotelluric sounding, as the depth to an electrically conducting, anisotropic layer can be well constrained, whereas the thickness of the layer cannot. The magnetotelluric technique is a passive technique that involves measuring fluctuations in the natural electric (**E**) and magnetic (**H**) fields in orthogonal directions at the surface of the Earth. The orthogonal components of the horizontal **E** and **H** fields are related via a complex impedance tensor, **Z**:

$$\begin{vmatrix} E_x \\ E_y \end{vmatrix} = \begin{vmatrix} Z_{xx} & Z_{xy} \\ Z_{yx} & Z_{yy} \end{vmatrix} \begin{vmatrix} H_x \\ H_y \end{vmatrix} \quad (1)$$

For a one-dimensional or two-dimensional Earth with x or y aligned along strike (direction of maximum conductance), the diagonal elements Z_{xx} and Z_{yy} are zero. Mathematically, a one-dimensional anisotropic Earth is equivalent to a two-dimensional Earth. Measured data rarely have zero diagonal impedance elements in any coordinate system, but can often be described by a 'superimposition (decomposition) model' in which the data are decomposed into a local, non-inductive response (commonly termed 'galvanic') owing to multi-dimensional heterogeneities with dimensions significantly less than the inductive scale length of the data and a regional inductive response to an underlying two-dimensional structure[12,13]. For data aligned in the (x', y') coordinate system of the regional

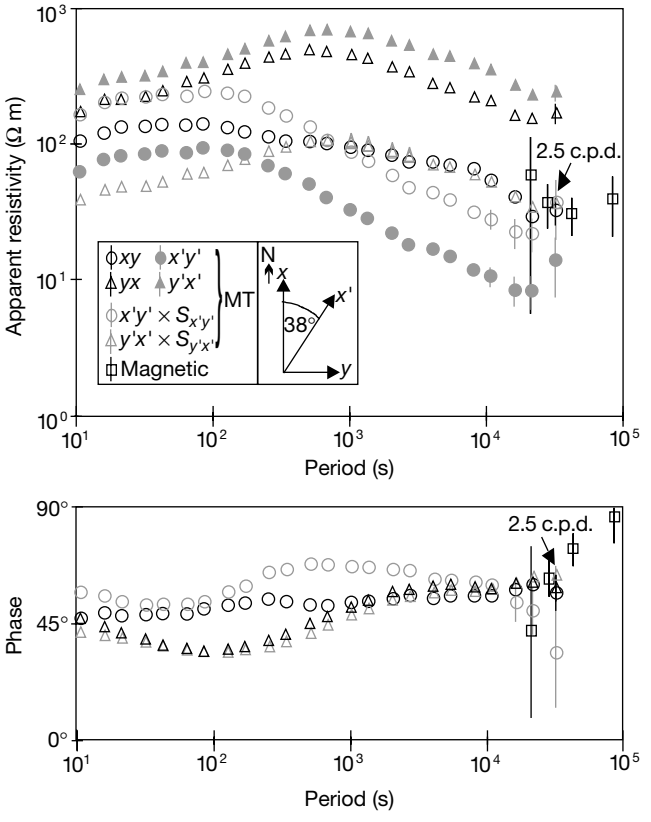

Figure 1 Apparent resistivity and impedance phases at station ASP before (x,y) and after rotation (x',y') and correction for static shifts. The magnetotelluric apparent resistivities are corrected for static shift by applying scaling factors $(S_{x',y'}, S_{y'x'})$ such that the magnetotelluric data at 2.5 c.p.d. correspond to the level of the magnetic transfer functions. Because the horizontal magnetic field induced by solar quiet (Sq) is strongly polarized in the east–west (y) direction, magnetic transfer functions can only be derived for the polarization corresponding to the xy polarization of the magnetotelluric data. There is, however, good correspondence between the yx magnetotelluric phases and the Sq phases. The phases are not affected by static shift, but are changed by rotation.